Hindawi
Advances in Civil Engineering
Volume 2018, Article ID 4785960, 10 pages
https://doi.org/10.1155/2018/4785960

Research Article

Laboratory and Centrifuge Model Tests on Influence of Swelling Rock with Drying-Wetting Cycles on Stability of Canal Slope

Chen Zhang[1,2] **Zheng-yin Cai**[1,2] **Ying-hao Huang**[1,2] **and Hao Chen**[1]

[1]*Nanjing Hydraulic Research Institute, Nanjing, China*
[2]*State Key Laboratory of Hydrology-Water Resources and Hydraulic Engineering, Nanjing, China*

Correspondence should be addressed to Zheng-yin Cai; zycai@nhri.cn

Received 14 June 2018; Revised 2 September 2018; Accepted 19 September 2018; Published 20 December 2018

Guest Editor: Yongfeng Deng

This study focused on the swelling behavior of swelling rock from canal basement under multiple drying-wetting (D-W) cycles. A series of laboratory tests were conducted on a swelling rock, with the cracking and strength behaviors investigated. By using image-processing technique, the crack patterns were described, and then quantitatively analyzed on the basis of the fractal dimension. The experimental data indicated that swelling ability, including cracking level, fractal dimension, and strength, decrease with increasing drying and wetting cycle. On this basis, a series of centrifuge model simulations for simulating slope failure by drying-wetting cycles were performed, where the drying process was achieved by heat bulbs. The monitoring results suggested that a global slope failure has occurred after total cycle of 4th corresponding to 4 years. Due to the development of surface cracking, the infiltration in the slope was severe and nonuniform in space and time. Meanwhile, the failure mechanism of soft rock slope induced by D-W was discussed.

1. Introduction

Swelling rocks contain silicate clay minerals that have the potential for swelling and shrinkage under changing moisture contents. Progressive deformation of the swelling rock can be caused during the drying-wetting (D-W) cycle, which may affect the safety of building foundations, tunnels, water canals, and liner and cover systems in waste containment facilities. The expansibility behavior of expansive soft rock has always been one of the major problems in damage to hydraulic infrastructure. For example, a water transfer project in Xinjiang area, with a large number of swelling mudstones distributed, slope failures, and local collapses (Figure 1), often occurs along the main canal. The canal damages caused by swelling rock reached approximately two-third of the annual damages reported, and the cost for repairing canal structures damaged by swelling mudstones accounted for 60% of the total annual maintenance cost.

A large number of swelling soil slope failure cases have been investigated, which were found to show some typical characteristics, such as shallow layer, tractive sliding, gentle motion type, and seasonal occurrence [1]. These characteristics are closely associated with the behavior of swelling soil. Therefore, many laboratory and in situ tests were conducted to study the phenomenon of swelling and shrinkage [2–5], D-W process [6–8], cracking in clay soils [9–12], and mechanical and hydraulic behaviors of expansive soils [13, 14]. However, comprehensive theory on failure mechanism and stability analysis methods of expansive soil slope are still insufficient due to the complex characteristics of swelling soil. Current engineering practices for determining the physicomechanical parameters of expansive rocks are mostly based on simplified laboratory tests or empirical equations. These practices may prone to mischaracterize the engineering characteristics, even result in a contradictory conclusion.

Commonly, the assessment of expansion potential was accomplished by one cycle of wetting in geotechnical practice. In some arid areas, the water is mainly from leakage, resulting in a long-term process under slow seepage and evaporation until slope failure, which is different from

(a) (b)

Figure 1: Typical slope failure of main canal in Xinjiang, China.

humid areas that are caused by drastic climate change in a short time. Nevertheless, for canal slope, due to the inevitable leakage, evaporation, rainfall, and other extreme climate conditions, it often has a more significant D-W boundary. Moreover, due to the limits of existing theory, hazardous working conditions, and the long-time scales of failure behavior, less academic attention has been paid on the issue of development of cracks and D-W cycles on stability of canal slope in arid areas. Recently, some innovative techniques, including image analysis [12, 15, 16] and fractal dimension analysis [17], have been used in soil-cracking studies. They were conducted on swelling soil to investigate the evolution of surface cracks, inner fractures, volume change, etc. Additionally, due to the characteristics of self-weight equality, the centrifuge-modeling technique has been used for examining the instability of expansive soil slope [18–21], and these studies provide reference for the full-scale landslide.

The objective of the present study is to investigate the swelling behavior of soft rocks in canal basement under cyclic moisture changes. For this purpose, two swelling rocks were obtained from the main canal of north Xinjiang water canals. After each cycle, the surface cracks and strength characteristics of swelling rocks were measured. A quantitative method was developed to characterize the crack patterns by combining the image processing with the fractal dimension concept. Additionally, the failure of swelling rock canal slope was investigated by centrifuge modeling.

2. Laboratory D-W Tests

In order to better understand cracking behavior and strength characteristics in swelling rocks from canal basement, a series of small specimen tests were carried out with two typical swelling rocks subjected to D-W, including crack observation test and direct shear test.

2.1. Preparation of Swelling Rock Specimens. The tested materials were prepared with two swelling rocks, which were taken from the construction field of a water transfer project in Xinjiang, a typical arid area in China. Compared with the "cyan mudstone" (CM), the swell potentials of the "yellow mudstone" (YM) are lighter than "cyan mudstone" where the names are based on apparent dominating color. The physical properties of the tested swelling rocks are listed in Table 1.

Considering the influence of density, swell potentials, and its' influences on strength of swelling rock under multiple D-W cycles, four test groups with different dry density and swelling potential were designed. Before preparation, swelling rocks were air-dried via mortar and pestle to reduce the size of the clay clods, and stored in buckets. In order to make the moisture equilibration, the remolded samples were prepared for 24 h to the optimal water content with 18.8% by CM and 14.75% by YM. The soil behavior is significantly affected by specimen size. In general, the physical soil model should be large enough to simulate the large cracks. However, the purpose, in this research, is to study the characteristics of cracks development and strength simultaneously under the D-W cycles. Therefore, the samples in crack observation tests and direct shear tests were prepared in the same size, which are 61.8 mm in diameter and 20 mm in thickness (standard size in direct shear test in CHN code [22]). The compaction tests showed that the maximum dry density of "natural CM" is close to 1.6 g/cm^3 and 1.8 g/cm^3 of "natural YM"; however, the degree of compaction of the prototype is about 90%. Based on this, the dry density of remolded samples had been designed as 1.8 g/cm^3, 1.6 g/cm^3, and 1.5 g/cm^3 in CM and 1.8 g/cm^3 in YM, respectively. Among them, the specimens of 1.6 g/cm^3 and 1.5 g/cm^3 were used to investigate the influence of density.

After solid pressing by one layer, the specimen surfaces were smoothed lightly with a grafter to obtain a uniform thickness. A thin layer of Vaseline was applied on the inner walls of the containers to reduce the boundary friction. The wetting process of the prepared cylindrical specimens was presented in vacuum saturation until the vacuum degree reached 95% (accuracy 0.1 g). After the completion of vacuum saturation, the specimen was exposed to the open environment (20°C ± 1.2°C without direct sunlight, and relative humidity 50% ± 10%) until the water was reduced to the residual moisture content. After the drying process completed, the sample was vacuum-saturated. To complete the D-W cycles, the aforementioned process was repeated. One battery consisted of five samples, four of which were used to observe cracks, and the remaining one was used for direct shear tests.

Table 1: Physical properties of tested materials.

Physical property	Value	
	CM	YM
Liquid limit, L_L (%)	61.3	57.1
Plastic limit, L_p (%)	20.1	17.6
Plasticity index, P_I	41.2	39.5
Percentage of clay (%)	30.1	32.5
Swelling ratio	88	74
CHCS classification	CH	

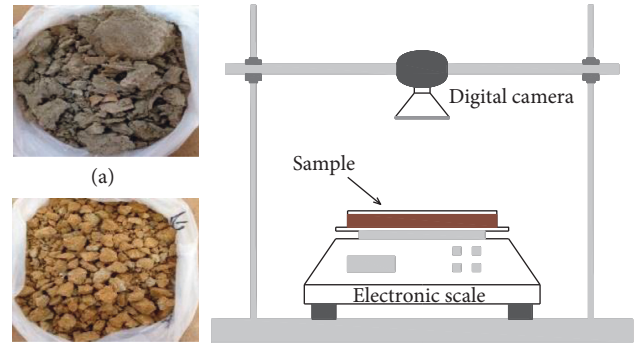

Figure 2: Using rocks and experimental set-up used for crack observation.

2.2. Observation of Crack Patterns. At the end of each D-W cycle, the surface of each specimen was pictured by using digital camera to capture the crack patterns. The camera lens was fixed parallel to the sample surface with a suitable distance to ensure the sample totally within the shooting range, as shown in Figure 2. Negative sources on image quality were minimized by blacking out the lab and illuminating the specimens by LED surrounding the container without camera flashlight. Every initial RGB images in each D-W cycle are shown in Figure 3. Now, a series of typical crack patterns after different D-W cycles are observed with different dry density and swelling ingredients. The distinct phenomenon is the development of surface fractures along with the increase of wetting and drying cycles. During the first D-W cycle, obvious cracks can be visually observed on the specimen surface with dry density of 1.8 g/cm^3 and 1.6 g/cm^3. On the one hand, ring-shaped cracks appear in specimens with dry density of 1.8 g/cm^3. After three cycles, more crack areas for all sampling compared to previous cycles. However, in the 4th cycle, the area seems no longer grown by visual inspection.

In order to analyze the geometric characteristics of cracking quantitatively, the digital image processing is launched by using MATLAB software. The initial RGB images of four specimens at the same dry density are wholly processed. It means that the shrinkage crack present around the specimen is included. The binary image of developing cracks on surface specimens are presented in Figure 3, where a function of "Graythresh" in the software is used in the image processing. It is easy to use the converted matrix to calculate the geometric parameters of the binary images, such as the fractal dimension and the surface crack ratio [23].

The box-counting dimension, D_b [24], is used in this study for fractal analysis; the number of square boxes intersected by the image, $N(s)$, and the side length of the squares, s, are also obtained where each image is covered by a sequence of grids of descending sizes and for each of the grids. The linear regression equation of $\log(N(s))$ against $\log(s)$ that used to estimate the fractal dimension is as follows:

$$\log(N(s)) = D_b \log(s) + A, \quad (1)$$

where the A is a constant; $N(s)$ is proportional to r^{-D_b}. D-W cycles for all specimens are depicted by solid line in Figure 4. The curves also demonstrate a decreasing trend in the crack with increasing number of D-W cycles, which well corresponds to the phenomenon of swelling clayey soils. As we know, during the air-drying processes, the action of the moisture gradient will lead to the stress redistribution with the tension of the upper part and the compression of the lower part. With the cracks gradually developed and finally covered on the whole sample surface, the moisture content of the surface and shallow layer of specimens gradually decrease. After rehydration, although the cracks close, the tensile strength at the position of cracks cannot be restored. This is the main reason for the expansion of cracks under repeated D-W cycles. On the contrary, the influence of dry density is not prominent; the fractal count of the sample with the density of 1.6g/cm^3 is higher than the sample with density of 1.5g/cm^3. Notice that the fractal count of 1.8 g/cm^3, before the 3rd cycle, is close to 1.6 g/cm^3. But it drops at the last two cycles. It is observed that the irregular net cracks on surface with dry density of 1.5 and 1.6 g/cm^3 are more than that of the sample of 1.8 g/cm^3; however, the main crack of sample with 1.8 g/cm^3 is the shrinkage crack which occurs at the side of the ring sampler, resulting in the relatively low level of irregular and chaotic degree of cracking, which is the essence of fractal dimension.

With the same dry density condition, the total fractal count of CM is higher than that of the yellow stone (although the count is almost close to the last two cycles). This was attributed to higher clay minerals occurring closer to the surface and higher swelling potentials for higher dry density. As previously described, the fractal dimension D_b can be used to evaluate the spatial distribution of cracks, the density of cracks, and the tendency of the crack traces to fill the area in which they are embedded. At least, the abovementioned result suggested that the interconnectivity of soft rock surface cracks is susceptible to the effects of density and mineral contents.

2.3. Strength Characteristics under D-W Cycles. A series of direct shear test was conducted to investigate the relationship between the strength and the crack patterns on multiple D-W cycles. All shear tests were carried out in each sample after the wetting process, under vertical loads of 50 kPa, 100 kPa, 200 kPa, and 300 kPa. The cohesion as well as the number of D-W cycles for each sample is also depicted in Figure 5 by a hollow wire. It can be seen that the computed fractal dimensions of the three clay samples during cyclic

Figure 3: Initial and binary images of three different samples at the ending of tests (1.8 g/cm^3, 1.6 g/cm^3, and 1.5 g/cm^3 of cyan mudstone and 1.8 g/cm^3 of yellow mudstone from top to bottom).

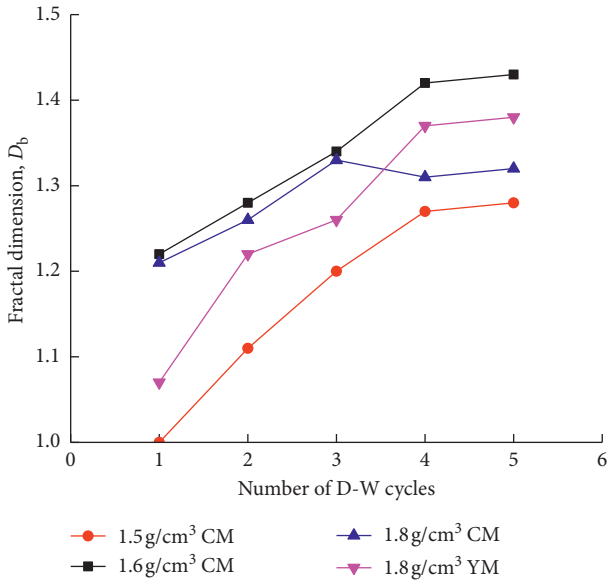

Figure 4: Variations of fractal dimension with the number of D-W cycles.

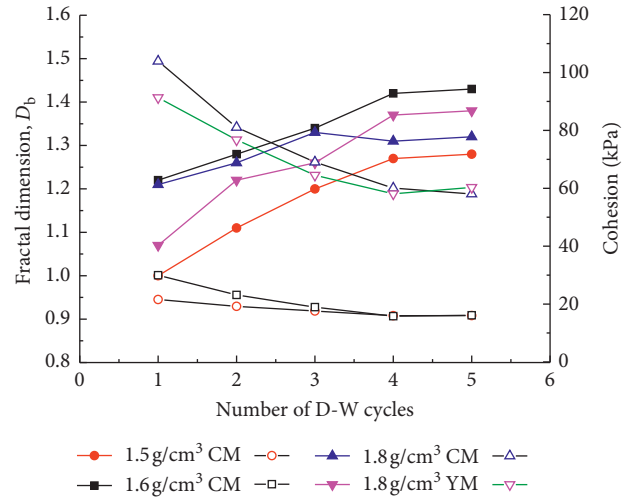

Figure 5: Variations of cohesion as well as fractal dimension with the number of D-W cycles.

drying-wetting are within the theoretically allowable range of 1.0 and 1.6. The fractal dimension of each sample increased with the increasing of D-W cycles until the corresponding shear strength decreased to its residual value. The shear strength of cyan mudstone samples with the dry density of 1.8, 1.6, and 1.5 g/cm^3 of CM and 1.8 g/cm^3 of YM were decreased approximately from 103 kPa, 30 kPa, 21.5 kPa, and 91 kPa to 58 kPa, 16.1 kPa, 15.9 kPa, and 60.2 kPa, respectively. The results in Figure 5 suggested that the successive D-W do not increase the development of cracks, but reduce the rock strength. However, this change begins to converge after the 4th cycle; it may be considered that if a canal which is filled with this soft rock is not damaged in 5 D-W cycles, the probability of failure will be greatly reduced in further cycles; in other words, the subsequent damage is not caused by a pure reduction in strength reduce and development of cracks. Similar to previous investigation about swelling clayey soil, the angle of friction of the soft rock remained more or less constant under D-W cycles (no longer given in this paper). The fractal dimension D_b can be used to evaluate the spatial distribution of cracks, the strength of cracks, and the tendency of the crack traces to fill the area in which they are embedded.

It is noted that the cohesion of CM and YM with the density of 1.8 g/cm^3 is much larger than that of other specimens. Some test results [25, 26] showed that the strength is slightly affected by the density. On the contrary, the effect of density on strength is obvious in this study. This tendency can also be demonstrated by the observed two test phenomena: (1) the initial strength level after first D-W cycle, and (2) decreasing amplitude of strength. However, in Figure 3, it can also be seen that the soil sample with a lower

density level shows more visible cracking, especially penetrating cracks on the sample surface after the first cycle. On the other hand, the fractal dimension D_b of the CM samples with a density of 1.6 g/cm^3 was always at a higher level in every D-W cycle, as the analysis of the fractal dimension is shown in Figure 5. This structural damage may strongly affect the shear test results and related to the soil properties and sample sizes.

3. Centrifuge Modeling

3.1. Slope Models and Testing Procedures. Due to the stress confinement, the centrifuge-modeling technique was used for examining slope instability and deformations of geological problems. As aforementioned, such long-time scales of the D-W process on canal slope in arid area request too much resource while field tests have been undertaken, but in centrifugal model, a reduced-scale model of lineal dimensions N^2 times smaller is used to simulate the full-scale problem under an acceleration N times the gravity. Thus, centrifuge modeling of such problems is an attractive proposition. With this aim in view, an experimental campaign has been initiated to investigate the performance of swelling rock slope subjected to D-W cycles by centrifuge modeling. According to the results of cracking test, the model soil were conducted on CM to obtain a dry density of 1.6 g/cm^3 for Model 1 and 1.5 g/cm^3 for Model 2, corresponding to the greater level of fractal dimension and lowest level, respectively. The model was constructed in a rigid container with inner dimensions of 680 mm × 350 mm × 450 mm (length × width × height). The model was prepared with initial water contents of 18.8%. After the hit-solid process, the slope was excavated to its final grade of 1 (V) : 2.5 (H) with a height of 100 mm. The finished slope was covered with plastic sheets and cured overnight before testing was conducted by introducing moisture to the slope surface. A video was placed in front of the slope in order to view the slope face during flight and the grid lines on the slope for measuring ultimate displacements. Eight miniature cylindrical pore pressure transducers (PPTs) that can measure a pressure from 0 to 350 kPa were embedded at different locations to observe the change in positive pore pressure during testing. The view of slope model and location of PPTS are depicted in Figure 6, in which P1 to P3 and P4 to P7 are placed at a parallel distance of 20 mm and 40 mm from the slope face, respectively.

Before the wetting process, the water was added to the phreatic line of 90 mm under 1 g to simulate the water in canal. A thick geo-cloth was laid on the bottom of the slope to prevent the impact of water splashing. The centrifuge took about 5 min to attain the targeted acceleration of 50 g, and then hold the acceleration under 50 g until the process terminated. The water in the canal model would be drained before the drying process. In order to provide a heat boundary, a battery of light bulbs at the top of the slope model was assembled upon 90 mm from the model surface to providing heat source for evaporation. The power of each bulb is 50 watt. The test was ended until the slope feature was observed in the video capture system. The test was performed by wetting the model for 90 mins and then drying the model for 220 mins. The required time was calculated as water supply and stop period of the prototype in accordance with N^2 times to the model scale 50. This time was approximately split in a 4-month/8-month ratio of the lengths of the wet and dry seasons in a year.

3.2. Testing Results. The seasonal D-W cycles have been shown to produce significant irrecoverable regional deformation below a slope in swelling rock. Figure 7 presents the ultimate slope failure in the lateral and vertical view. It can be seen that a large number of spots scattered on the surface after slope failure, and the failures in two models are the same as global and lateral fail. During the test, it was found out that slope failure occurred not instantaneously, a significant progressive failure was observed for this slope. No exception the failure occurs within 5 D-W cycles that typically occurred right after the 5th cycle in Model 1 and the 4th cycle in Model 2, corresponding to 5 years and 4 years in the prototype, respectively. At least, it indicated that the degree of soft rock slope failure originates in mineralogical composition and content. The tensile crack could be observed at the top of slope in two tests, which in Model 2 is more obvious than in Model 1. In Model 2, the width of the crack is approximately 3 mm in horizontal and 5 mm in vertical direction. The displacement was in calculating for the final height which was obtained as grid lines. The location of maximum displacement of two models is presented in the vector diagram of slope feature in Figure 8. The displacement trend of two models is close. By multiplying the height by the gravity at failure, the maximum displacement of slope is up to 1.3 m and 1.4 m, respectively.

Figure 9 shows the variation of measured pore pressure within Model 1 at the onset of seepage for model slope. In the first wetting process, the PPT did not record significant change in pore pressure except P1, which is located at the upper portion of slope bottom; this was because of the fact that the precipitation did not infiltrate to a depth where they are located. However, during the next period of the wetting process, with the development of desiccation cracking in the prior drying process, water fills the cracks and fissures; in addition to increasing the hydrostatic forces, the water is slowly absorbed by the swelling rocks. In the 3rd cycle, the P1, P2, and P3 which are located at the upper portion of the slope were recorded. After 5 cycles, all PPTs were recorded except P4, which is located near the top slope under the surface of 40 mm from the vertical of slope line. Besides, it can be seen that, from 3 to 5 cycles, the pore pressure started to increase with the acceleration. It indicated that, due to the effect of fracture develops, the water directly penetrated to the location of PPT at the beginning of the wetting process. Another phenomenon is no significant increase in pore pressure has been observed. The excess pore pressure was not responded to the slope failure. Owing to the limited space in model, enough PPTs were not installed to monitor the infiltration process with model time.

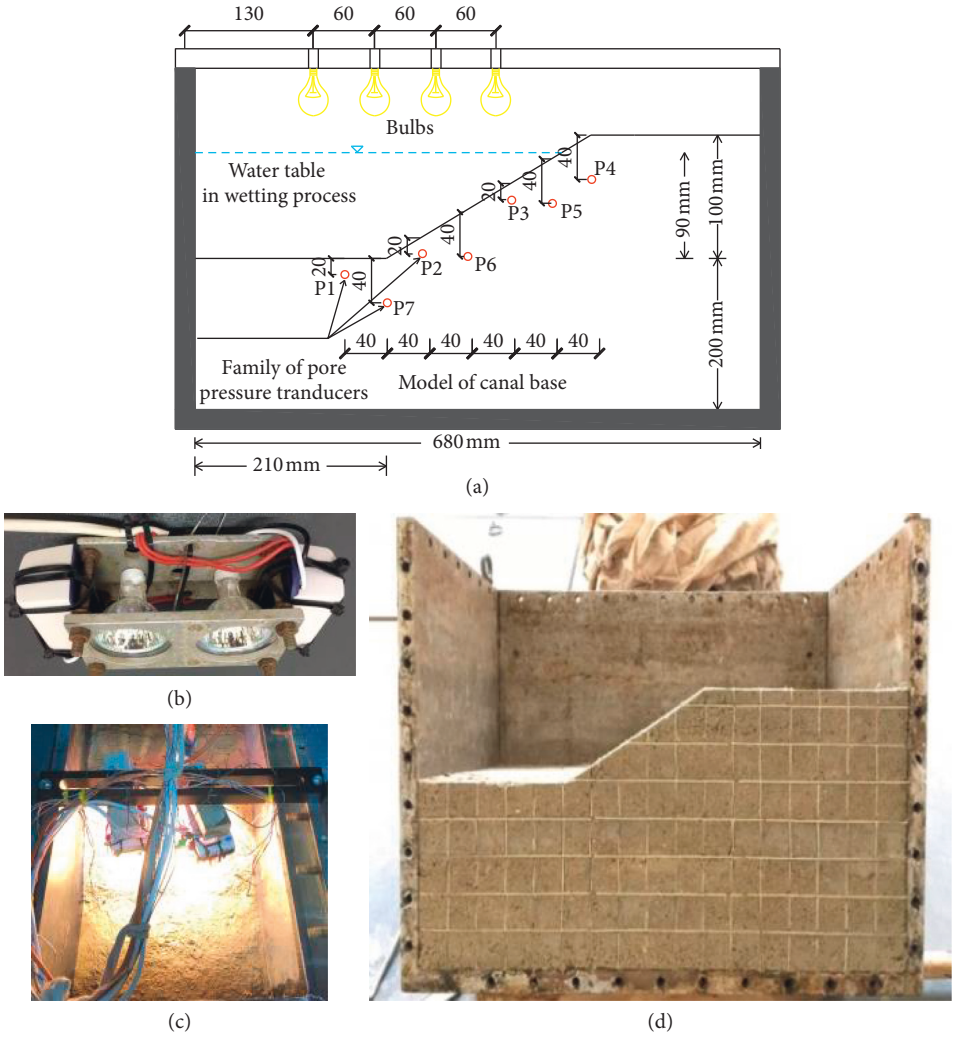

Figure 6: Centrifuge modeling of canal slope using bulbs (not to scale).

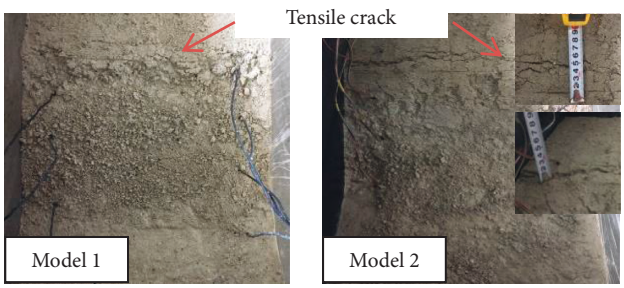

Figure 7: Vertical view of model surface after slope failure.

Figure 10 shows the "infiltration region" in two tests, which is an alternative strategy for the reflection of infiltration in swelling rock slope. Basing on the average value of PPTS in the stable phase (the saturation of the region is judged by comparing the reading with the hydrostatic pressure at the corresponding position), the region of 1st and 2nd cycles can be estimated. It was founded that the depth of

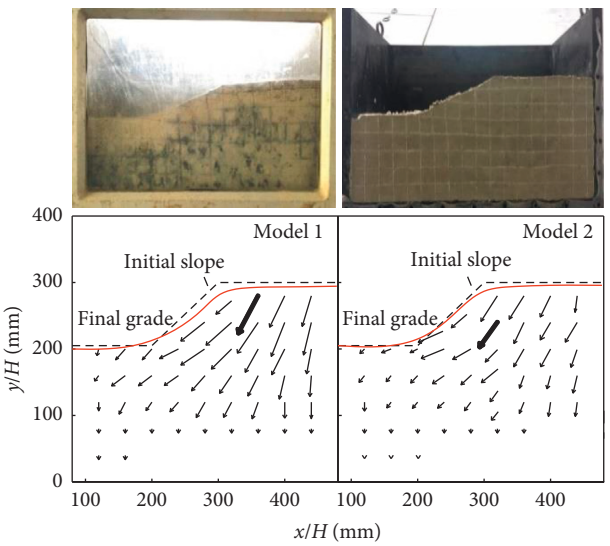

Figure 8: Slope failure and ultimate vector of displacements.

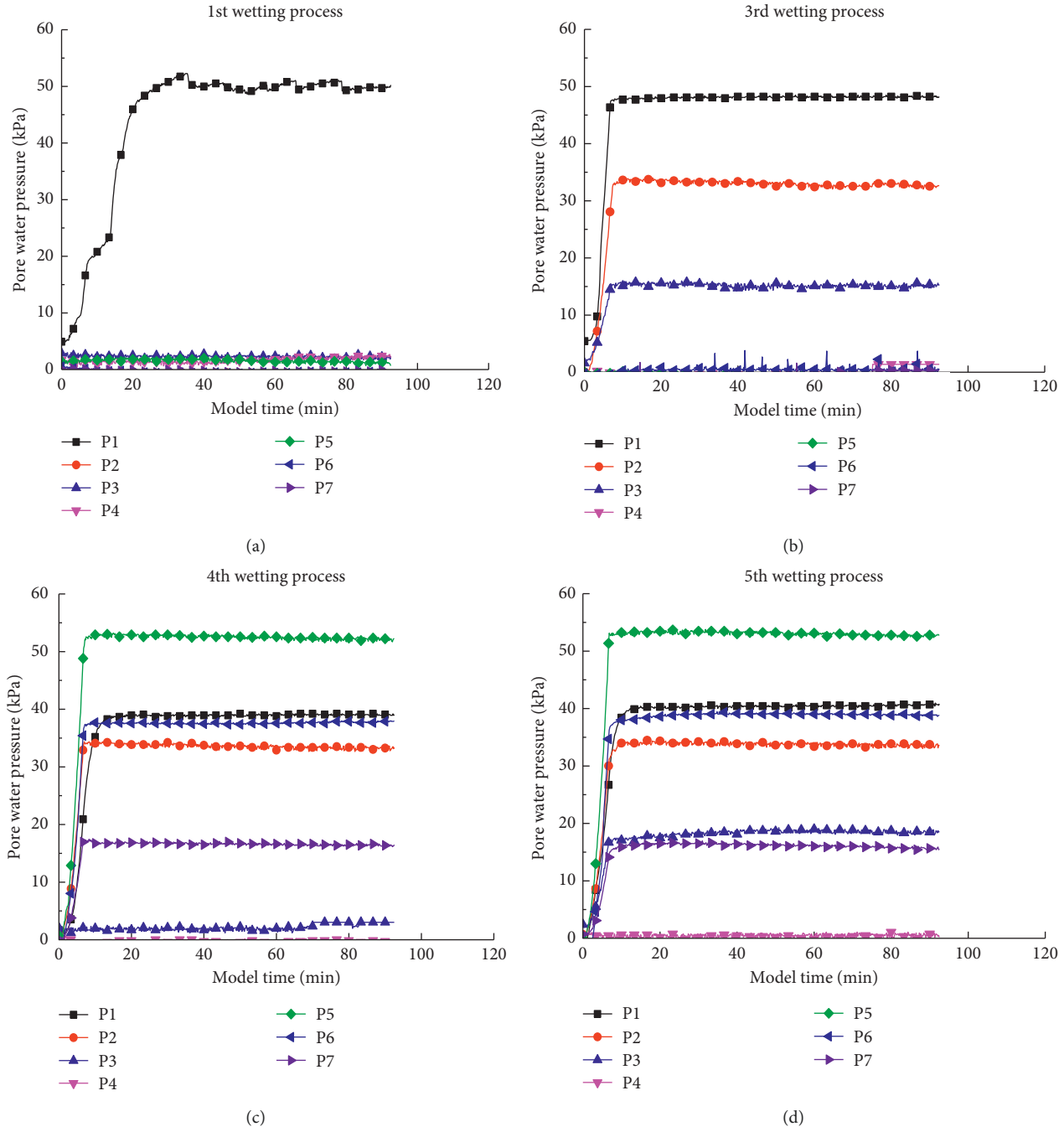

Figure 9: Variation of pore water pressure with model time.

the infiltrating area can reach 20 mm (with model scale) vertical below the surface for the first cycle in Model 1 without cracking, and similarly reach to 24 mm in Model 2. Due to the development of cracking, after 3 cycles, the infiltration region has reached to 40 mm below the surface in Model 1 and 50 mm in Model 2, respectively. In addition to monitoring the degree of region under infiltration, the saturation data recorded at the end of tests are presented in Figure 10. It can be seen that the regions were eventually extended to 44 mm in Model 1 and 53 mm in Model 2. The distribution of the saturate region is mainly near the surface and larger in toe and bottom, which is related to the depth of crack, hydrostatic force, and centrifugal acceleration. This accumulation of infiltration led eventually to the onset of progressive failure from the surface to inner surface, resulting in a large region of softening.

In the interval of each cycle, the cracks were depicted by plastic film on model surface of slope, as much as possible. Limited to space, the development of cracks on model surface in test 1 is given in Figure 11, with obvious cracking after every cycle which is depicted by pen. Owing to the existence of these cracks under circumstance of D-W cycles,

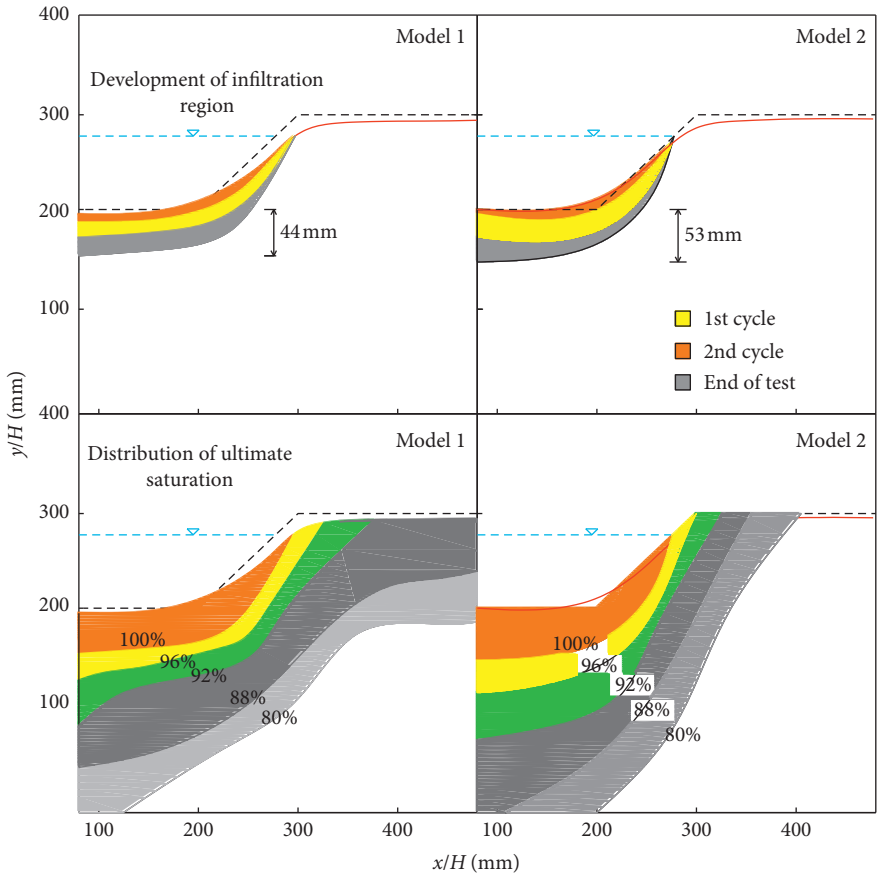

Figure 10: The development of "infiltration region" and ultimate distribution of saturation in models.

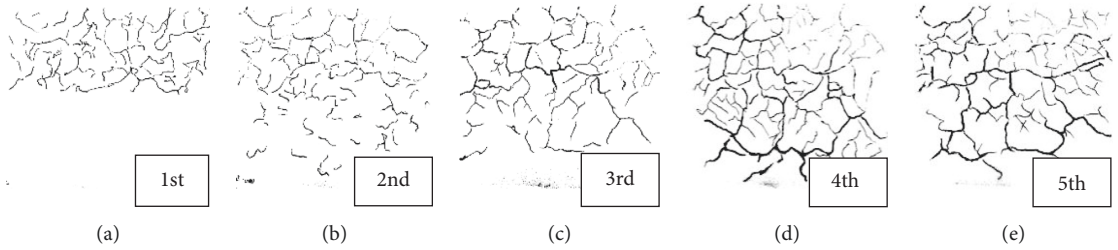

Figure 11: Depiction of surface cracks at the end of each D-W cycles in Model 1.

the canal suffered devastating damage after several years of coming into use. As the laboratory D-W tests showed, the seasonal shrinking and swelling behavior of the cracked clay zone results in a progressive reduction of the bulk shear strength of the swelling rock to the point where it may approach its residual strength. In centrifugal model test, the effect of the absorbed water is to increase the unit weight of clay as well as to decrease its shear strength. These mechanisms result in a simultaneous increasing in the sliding forces of slope and decrease in the resisting forces which are presented by centrifugal force. However, some previous research noted that cracking and hydraulic conductivity of swelling clay or rocks are controlled by plasticity and swelling [27]. The slope basement with highly swelling potential may enhance the effect of infiltration, and then aggravate slope failure. Although the results of laboratory D-W tests show that residual strength can still reach a safe conclusion by limit equilibrium slope stability methods, the maximum available shear strength on the base of each of the vertical slices may not be invoked for such swelling slopes.

In fact, the method of using bulbs for heating requires control of ambient temperature and humidity and requires rigorous math-physical methods to analyze testing results. Nevertheless, compared with the previous studies, one-time scale was carried out in this test that avoids the situation of mismatching of time. As far as the wreck mode of the canal slope is concerned, the centrifuge modeling has examined the lateral global failure about soft rock slope in relation to the hydric and evaporation due to climate and situation of

seasonal water delivery, which is associated with cracking, infiltration, swelling, and strength reduction.

4. Conclusions

A series of crack observation tests and direct shear tests were conducted on the remolded soft rock subjected to dry-wetting cycles, and a centrifuge modeling is presented herein for simulating full-scale slope failure induced by D-W cycles. The conclusions are as follows:

(1) The fractal dimension D_b was used to quantitatively analyze the degree of cracking of the specimens under cyclic D-W. The fractal analysis showed that the fractal dimension D_b is related to the dry density and swelling potentials, finally related to the swelling composition of soft rock.

(2) The cohesion decreases with increasing D-W cycles. After 4 cycles, the variation of cohesion changed in a negligibly small manner. The strength reducing is accompanied with cracking and will almost no longer develop until cracking converges to be stable.

(3) The centrifuge test results showed that at least four D-W cycles under the 50 g with true time of 4 years led to slope failure, which was the type of global and lateral failure without significant excess pore pressure. Both dry density level and D-W accumulation affected soft rock slope instability.

The relationship between fractal dimension and strength in laboratory tests and quantitative evaporation process in centrifuge modeling will be emphasized in subsequent studies.

Data Availability

The data used to support the findings of this study are included within the article.

Conflicts of Interest

The authors declare that they have no conflicts of interest.

Acknowledgments

This work was supported by the "National Key Research and Development Program of China" (Grant No. 2017YFC0405100), the "National Natural Science Foundation of China" (Grant Nos. 51709185 and 51879166), and the "Technical demonstration project of China Ministry of water Resource of the People's Republic of China" (Grant. No. SF-201704). It was also a part of work in the project funded by the Fundamental Research Funds for the Central Scientific Research Institute (Grant No. Y318001).

References

[1] D. Rosenbalm and C. E. Zapata, "Effect of wetting and drying cycles on the behavior of compacted expansive soils," *Journal of Materials in Civil Engineering*, vol. 29, no. 1, article 04016191, 2016.

[2] F. H. Chen, "Foundations on expansive soils," in *Developments in Geotechnical Engineering*, vol. 54, pp. 20–40, Elsevier, Amsterdam, Netherlands, 1988.

[3] A. A. Basma, A. S. Al-Homoud, A. I. Husein Malkawi, and M. A. Al-Bashabsheh, "Swelling-shrinkage behavior of natural expansive clays," *Applied Clay Science*, vol. 11, no. 2–4, pp. 211–227, 1996.

[4] H. Péron, L. Laloui, T. Hueckel, L. Hu et al., "Experimental study of desiccation of soil," in *Proceedings of Unsaturated Soils*, vol. 189, pp. 1073–1084, Carefree, Arizona, April 2006.

[5] A. J. Puppala, B. Katha, and L. R. Hoyos, "Volumetric shrinkage strain measurements inexpansive soils using digital imaging technology," *Geotechnical Testing Journal*, vol. 27, no. 6, article 12069, 2004.

[6] J. M. Fleureau, J. C. Verbrugge, A. G. Correia, P. J. Huergo, and S. Kheirbek-Saoud, "Aspects of the behaviour of compacted clayey soils on drying and wetting paths," *Canadian Geotechnical Journal*, vol. 39, no. 6, pp. 1341–1357, 2002.

[7] F. Yazdandoust and S. S. Yasrobi, "Effect of cyclic wetting and drying on swelling behavior of polymer-stabilized expansive clays," *Applied Clay Science*, vol. 50, no. 4, pp. 461–468, 2010.

[8] H. Nowamooz and F. Masrouri, "Influence of suction cycles on the soil fabric of compacted swelling soil," *Comptes Rendus Geoscience*, vol. 342, no. 12, pp. 901–910, 2010.

[9] P. C. Knodel, A. E. Dif, and W. F. Bluemel, "Expansive soils under cyclic drying and wetting," *Geotechnical Testing Journal*, vol. 14, no. 1, pp. 96–102, 1991.

[10] R. Ayad, J. M. Konrad, and M. Soulié, "Desiccation of a sensitive clay: application of the model CRACK," *Canadian Geotechnical Journal*, vol. 34, no. 6, pp. 943–951, 1997.

[11] C. S. Tang, Y. J. Cui, A. M. Tang, and B. Shi, "Experiment evidence on the temperature dependence of desiccation cracking behavior of clayey soils," *Engineering Geology*, vol. 114, no. 3-4, pp. 261–266, 2010.

[12] C. S. Tang, Y. J. Cui, B. Shi, A.-M. Tang, and C. Liu, "Desiccation and cracking behaviour of clay layer from slurry state under wetting– drying cycles," *Geoderma*, vol. 166, no. 1, pp. 111–118, 2011.

[13] J. H. Li and L. M. Zhang, "Study of desiccation crack initiation and development at ground surface," *Engineering Geology*, vol. 123, no. 4, pp. 347–358, 2011.

[14] M. Fernandes, A. Denis, R. Fabre, J.-F. Lataste, and M. Chrétien, "In situ study of the shrinkage- swelling of a clay soil over several cycles of drought- rewetting," *Engineering Geology*, vol. 192, pp. 63–75, 2015.

[15] H. Wang, J. Siopongco, L. J. Wade, and A. Yamauchi, "Fractal analysis on root systems of rice plants in response to drought stress," *Environmental and Experimental Botany*, vol. 65, no. 2-3, pp. 338–344, 2009.

[16] W. Tang and Y. Wang, "Fractal characterization of impact fracture surface of steel," *Applied Surface Science*, vol. 258, no. 10, pp. 4777–4781, 2012.

[17] Y. Lu, S. H. Liu, L. P. Weng, Z. Li, and L. Xu, "Fractal analysis of cracking in a clayey soil under freeze–thaw cycles," *Engineering Geology*, vol. 208, pp. 93–99, 2016.

[18] L. Nova-Roessig and N. Sitar, "Centrifuge model studies of the seismic response of reinforced soil slopes," *Journal of Geotechnical and Geoenvironmental Engineering*, vol. 132, no. 3, pp. 388–400, 2006.

[19] M. Kitazume and T. Takeyama, "Centrifuge model tests on influence of slope height on stability of soft clay slope," in *Proceedings of Geo-Congress*, pp. 2094–2097, San Diego, CA, USA, March 2013.

[20] H. Ling and H. I. Ling, "Centrifuge model simulations of rainfall-induced slope instability," *Journal of Geotechnical and Geoenvironmental Engineering*, vol. 138, no. 9, pp. 1151–1157, 2012.
[21] W. A. Take and M. D. Bolton, "Seasonal ratcheting and softening in clay slopes, leading to first-time failure," *Géotechnique*, vol. 61, no. 9, pp. 757–769, 2011.
[22] Standard for Soil Test Method, GB/T 50123-1999, in Chinese.
[23] F. K. Decarlo and N. Shokri, "Effects of substrate on cracking patterns and dynamics in desiccating clay layers," *Water Resources Research*, vol. 50, no. 4, pp. 3039–3051, 2014.
[24] H. O. Peitgen, H. Jürgens, and D. Saupe, *Chaos and Fractals: New Frontiers of Science*, Springer, Berlin, Germany, 2004.
[25] W. H. Liu, Q. Yang, X. W. Tang et al., "Mechanical behaviors of soils with different initial dry densities under drying-wetting cycle," *Journal of Hydraulic Engineering*, vol. 45, no. 3, pp. 261–268, 2014, in Chinese.
[26] B. Xu, Z. Z. Yin, and S. L. Liu, "Experimental study of factors influencing expansive soil strength," *Rock and Soil Mechanics*, vol. 32, no. 1, pp. 44–50, 2011, in Chinese.
[27] M. H. T. Rayhani, E. K. Yanful, and A. Fakher, "Physical modeling of desiccation cracking in plastic soils," *Engineering Geology*, vol. 98, no. 1-2, pp. 25–31, 2008.